NASA-CR-120891

TRW ER-7451

INTERACTIONS BETWEEN CREEP, FATIGUE AND STRAIN AGING IN TWO REFRACTORY ALLOYS

TOPICAL REPORT No. 2

Prepared for

NATIONAL AERONAUTICS AND SPACE ADMINISTRATION
LEWIS RESEARCH CENTER
UNDER CONTRACT NAS 3-6010

TRW ***MATERIALS TECHNOLOGY LABORATORIES***

CLEVELAND, OHIO

CAT. 17

Request for copies of this report should be referred to

National Aeronautics and Space Administration
Office of Scientific and Technical Information
Attention: AFSS-A
Washington, D. C. 20546

1. Report No.	2. Government Accession No.	3. Recipient's Catalog No.
NASA-CR-120891		

4. Title and Subtitle	5. Report Date
INTERACTIONS BETWEEN CREEP, FATIGUE, AND STRAIN AGING IN TWO REFRACTORY ALLOYS	February 1972
	6. Performing Organization Code

7. Author(s)	8. Performing Organization Report No.
K. D. Sheffler	TRW ER-7451
	10. Work Unit No.

9. Performing Organization Name and Address	11. Contract or Grant No.
TRW Inc. Materials Technology Laboratory 23555 Euclid Avenue Cleveland, Ohio 44117	NAS 3-6010
	13. Type of Report and Period Covered
12. Sponsoring Agency Name and Address	Contractor Report
National Aeronautics and Space Administration Washington, E.C. 20546	14. Sponsoring Agency Code

15. Supplementary Notes

Project Manager, P. E. Moorhead - Materials and Structures Division
NASA Lewis Research Center
Cleveland, Ohio 44135

16. Abstract

The application of low-amplitude, high-frequency fatigue vibrations during creep testing of two strain-aging refractory alloys (molybdenum-base TZC and tantalum-base T-111) significantly reduced the creep strength of these materials. This strength reduction caused dramatic increases in both the first stage creep strain and the second stage creep rate. The magnitude of the creep rate acceleration varied directly with both frequency and A ratio (ratio of alternating to mean stress), and also varied with temperature, being greatest in the range where the strain-aging phenomenon was most prominent. It was concluded that the creep rate acceleration resulted from a negative strain rate sensitivity which is associated with the strain aging phenomenon in these materials. (A negative rate sensitivity causes flow stress to decrease with increasing strain rate, instead of increasing as in normal materials.) By combining two analytical expressions which are normally used to describe creep and strain aging behavior, an expression was developed which correctly described the influence of temperature, frequency, and A ratio on the TZC creep rate acceleration.

17. Key Words (Suggested by Author(s))	18. Distribution Statement
Creep Fatigue Interactions	Unclassified - Unlimited

19. Security Classif. (of this report)	20. Security Classif. (of this page)	21. No. of Pages	22. Price*
Unclassified	Unclassified	25	$3.00

* For sale by the National Technical Information Service, Springfield, Virginia 22151

FOREWORD

The work described in this report was performed under National Aeronautics and Space Administration Contract NAS 3-6010. The purpose of the study was to obtain fatigue life data on refractory alloys for use in designing space power systems. The program is under the direction of Paul E. Moorhead, Technical Manager for the Space Power Systems Division of NASA-Lewis Research Center.

Prepared by: K. D. Sheffler
K. D. Sheffler
Engineer

Reviewed by: H. E. Collins
H. E. Collins
Principal Engineer

Approved by: E. A. Steigerwald
E. A. Steigerwald
Manager
Materials Research Department

INTRODUCTION

A recent study has shown that significant alterations could be made to the creep behavior of a molybdenum alloy (TZC) by the application of low amplitude, high frequency fatigue vibration during creep (1). These tests indicated that moderate variations of the applied load (±45%) at a frequency of about 19 KHz would cause the creep rate to increase by as much as two orders of magnitude over that obtained under static stress at the same peak values. These results are significant since many turbine applications involve stress conditions where a high frequency dynamic flutter load is superimposed on a steady centrifugal force. On this basis, conventional creep data obtained at the peak stress condition would result in design predictions that would be almost two orders of magnitude less than that experienced when a dynamic load of ±45% was applied. In more recent tests, a similar effect has been found in a tantalum alloy (T-111). These later tests also showed that the effect extended to load variations as small as ±10% in both materials, and to frequencies as low as 10 KHz in TZC. Details of these new findings are reported in this paper, together with a possible interpretation of the responsible mechanism.

EXPERIMENTAL DETAILS

The T-111 alloy was tested in the form of 0.600 inch plate cold rolled and recrystallized 1 hour at 3000°F (1649°C). Chemical analysis of this plate is given in Table 1, while light and electron micrographs are shown in Figures 1 and 2. Although the structure appears clean at optical magnifications, a small precipitate can be seen in the electron microscope. Electron probe emission and distribution scans showed that the precipitate was hafnium oxide. The microstructure was similar to that of the recrystallized 0.030 inch T-111 sheet tested in a companion ultrahigh vacuum program (2), except that in the sheet material the hafnia precipitates were found to be distributed preferentially at the grain boundaries.

The TZC material tested in this program was forged plate which was recrystallized 1 hour at 3092°F (1700°C). Compositions of the TZC test materials are shown in Table 2, and an optical photomicrograph of the recrystallized TZC alloy is shown in Figure 3. The discrete carbide precipitates typical of this material are readily apparent even at the 250X magnification. The 2000°F (1093°C) tensile properties of both the TZC and the T-111 alloys are listed in Table 3.

To eliminate the possibility of environmental contamination all of the tests were conducted in ultrahigh vacuum chambers at pressures less than 1×10^{-7} torr. The detailed design and operation of the test systems have been previously discussed (1). Briefly, the apparatus consisted of an ion pumped ultrahigh vacuum chamber containing a resonant load train driven from the top by a PZT piezoelectric transducer and loaded from the bottom through a bellows-sealed coupling. The specimen was heated by a tantalum resistance

element, and specimen temperature was measured with a W-3%Re/W-25%Re thermocouple located adjacent to the gauge section. Specimen extensions were measured optically using a traveling telescope sighted onto the specimen through a quartz window in the chamber wall.

The test procedure involved pumping the chamber to a pressure below 1×10^{-6} torr, followed by heating slowly enough so that the pressure never rose above that value. The specimen was held at temperature until the chamber pressure was below 1×10^{-7} torr, after which the sample was loaded to the mean stress and allowed to creep until a stable condition was achieved. At the temperatures and loads involved, the creep rate dropped to very low values ($\sim 10^{-8}$/hour) after a short time. The high frequency drive was then applied and a minor temperature adjustment was made to compensate for a slight heating produced by the drive. After a stabilization period of about one-half hour the exact dynamic strain was measured using an optical cathetometer having a veriner filar eyepiece calibrated to ±5μin. A characteristic surface marking was selected on the machined surface and a minimum of ten measurements of the size of the marking were made both before and after the application of the high frequency drive. (In every case, enough measurements were made to reduce the standard deviation on the measurement below ±10μin.) The dynamic displacement was then determined from the difference in the surface marking produced by the ultrasonic drive. This was converted to total dynamic strain range by dividing by the distance of the surface marking from the center of the gauge section. The corresponding dynamic stress range was calculated using the known dynamic modulus for each material. Drive was continued until a fatigue crack was initiated, until 5% dynamic

creep occurred, or until 10^{10} cycles were accumulated (about 150 hours). Creep measurements were made periodically throughout the tests with the optical cathetometer.

Tests were performed at 1800, 2000, and 2200°F (983, 1093, and 1204°C) over a range of loads and A ratios (ratio of alternating to mean stress, see Figure A-2). The present study concentrated on the lower A ratio range (0.1-0.25) as being more pertinent to meaningful design problems. Although the majority of experiments were conducted at a nominal frequency of 19 KHz, selected tests were also made on TZC at 15 and 10 KHz to evaluate the effect of this variable on the fatigue-creep behavior.

RESULTS

Typical creep behavior of TZC alloy with superimposed high frequency fatigue stress is shown in Figure 4a, while the fatigue-creep behaviors of both alloys are summarized schematically in Figure 4b. Marked creep rate increases occurred in both alloys upon application of the high frequency vibration, and this acceleration resulted in a significant increase in the first stage creep strain. The first stage creep behavior was remarkably similar in the two materials, as illustrated in Figures 5 and 6*. It was dependent on both stress and A ratio, but appeared to be relatively independent of temperature. In most cases the first stage creep was between one and two orders of magnitude higher than corresponding isostatic primary creep extensions at the same integrated stress value.

Figure 4 illustrates that the high frequency fatigue-creep rate acceleration was continued into second stage in the TZC alloy. It was also observed that the TZC acceleration could be "turned off" and "turned on" almost instantaneously simply by removal and re-application of the dynamic drive. An important corollary observation was the absence of the large first stage extension upon re-application of the drive. This immediate response indicates that the mechanism responsible for the high frequency creep rate acceleration in TZC involves short range, reversible atomic rearrangements rather than permanent, long range diffusion controlled structural

---

* The integrated stress referred to throughout this paper is essentially a mean stress value which has been adjusted upward slightly to account for the relatively small creep rate acceleration caused by the non-linear dependence of creep rate on stress. See Appendix A for a more detailed discussion of this point.

alterations. This conclusion is also supported by the observation that high-frequency fatigue testing caused essentially no change in the TZC microstructure, as indicated in Figure 7.

The experimental TZC creep rate data, which are summarized in Figure 8, indicate that the creep rate acceleration was dependent on both temperature and A ratio. The acceleration was largest at 1800°F (982°C) and was relatively small at 2200°F (1204°C). The acceleration increased with A ratio, but appeared to approach a limiting value at each temperature. The acceleration in TZC was also frequency dependent (Figure 9), being lower at 15 and 10 KHz than at 19 KHz.

Figure 4 illustrates that the high frequency creep rate acceleration was also continued into the second stage in the T-111 alloy. However, unlike the TZC material, the T-111 creep rate showed only a slight decrease when the high frequency drive was removed. It was also observed that the T-111 second stage high frequency fatigue-creep rates were comparable to the isostatic second stage creep rates (Figure 10) which were measured in T-111 alloy after the isostatic creep rate transition which is illustrated in Figure 4. Before this behavior can be discussed further it is necessary to provide background information concerning the conventional creep behavior of T-111 alloy.

The nominal composition of T-111 is Ta-8%W-2%Hf. Although T-111 depends primarily on solid solution strengthening for its high temperature properties, it has been shown that strain aging can also provide a significant strength contribution in the 1200 to 2200°F (649 to 1204°C) range (2). The strain-aging mechanism has been associated with a reactive metal-interstitial atom interaction, and activation energy measurements identified oxygen as the

interstitial atom species involved. The creep strengthening was particularly effective at very low strains (~.1%) but gradually lost its effectiveness at higher strain levels (between ~.2% and 1%). This behavior caused a creep rate transition to occur in T-111 of the form illustrated in Figure 4. The previous work showed that the isostatic creep rate transition resulted from a loss of oxygen which gradually depleted the interstitial atom specie associated with the strain age strengthening.

With this background information in view, the difference between the TZC and T-111 high frequency fatigue-creep behaviors can be explained by showing that the high frequency fatigue stress accelerated the deoxidation process. Evidence for the accelerated deoxidation was found in examination of the microstructure and composition of the fatigue tested specimens. Electron micrographs of T-111 in the tested condition (Figure 11) show a refinement of the structure by removal of hafnia as compared to as-received (Figure 2), which is similar to the refinement which resulted from isostatic ultrahigh vacuum creep testing. A significant oxygen loss was also measured in the fatigued samples, which is consistent with the observed structural refinement. Post-test oxygen levels were generally near 10 ppm, as compared with 100 ppm before test.

DISCUSSION

This discussion is based on the hypothesis that the high frequency fatigue-creep rate acceleration was caused by a negative strain rate sensitivity which has been found in TZC alloy by Raffo (3), and in T-111 alloy by Sheffler, et al (2). The importance of the negative rate sensitivity is that it causes flow stress to decrease with increasing rate, instead of increasing as in normal materials. Since the high frequency fatigue test involves extremely high strain rates, it follows that the effective flow stress of a strain rate softening material must decrease during this type of test. It is proposed that this strength reduction was the cause for the observed creep rate accelerations. Support for this hypothesis will be developed by a direct comparison of high frequency fatigue-creep rates with conventional creep test data. Because compositional changes occurred in T-111 which eliminated the acceleration in creep, the analysis will be confined to explaining the experimental observations obtained with the TZC alloy.

It will be assumed that there is no basic difference between the mechanisms of acceleration in the first and second stages of creep. This type of assumption has been supported in two separate studies of four different materials (stainless steel, nickel, zinc, and iron), both of which showed that the two stages are directly related to one another (4,5). It is supported in the present case by the similarity between the influence of A ratio on the ε_1 and $\dot{\varepsilon}_2$ parameters in TZC (compare Figures 5 and 8).

The strain rate softening hypothesis can be described analytically using the expresion given by Lubahn and Felgar (6) to relate flow stress (σ_f) to strain rate ($\dot{\varepsilon}$):

$$\sigma_f = K\dot{\varepsilon}^n \qquad (1)$$

where K is a constant and n is defined as the strain rate sensitivity. In the high frequency fatigue test $\dot{\varepsilon}$ becomes extremely high for a short time during each fatigue cycle (values as high as 2000 in/in/min. have been achieved, see Figure A-1), and if n is negative this causes a transient decrease in σ_f. This strength decrease causes a significant creep rate increase during a portion of each fatigue cycle, which results in a net increase in the experimentally measured average creep rate.

To test this hypothesis, the creep rate acceleration was defined analytically as the ratio of the high frequency fatigue creep rate to the isostatic creep rate at an equivalent integrated stress. The creep rate data in Figure 8 were used to calculate numerical values of the creep rate acceleration, and the influence of the experimental variables on these values was examined to see if it was consistent with the theory. Analytical treatments were also used to demonstrate that the acceleration values could be calculated by incorporating expression (1) into a conventional creep rate equation of the form:

$$\text{creep rate} \propto \sigma^N e^{-\frac{(\Delta H + V\sigma_f)}{RT}} \qquad (2)$$

where σ is applied stress, N is the stress exponent, ΔH is activation energy, V is activation volume, R is the universal gas constant, and T is the absolute temperature. Details of this analysis are presented in Appendix B.

Figures 12 through 14 show the influence of frequency, A ratio, and temperature on the creep rate acceleration. The results in Figures 12 and 13 show that both of the experimental parameters which directly influence the instantaneous strain rate (i.e., frequency and A ratio) also directly influence the acceleration values, which is consistent with the theory. Figure 14 shows that the influence of temperature on the strain rate sensitivity and on the acceleration effect is also consistent with the theory; that is, as the n value becomes less negative, the acceleration decreases.

Figures 12 through 14 also show that the calculated accelerations are in reasonable agreement with the experimental data. It should be emphasized that the calculated results were all obtained from a single equation relating the acceleration to frequency, temperature and A ratio, rather than from separate expressions for each parameter. It should also be emphasized that this expression was not simply the result of a curve fitting process, but was developed by the direct marriage of expressions commonly used for creep and for strain rate sensitivity. It is felt that the ability to develop a single relationship in this way, which will properly describe the influence of all three experimental variables on the creep rate acceleration, lends support to the basic strain rate softening hypothesis as the cause for the creep acceleration effects observed in the dynamic tests.

SUMMARY

Elevated temperature, high frequency, low amplitude, tension-tension fatigue tests were conducted on molybdenum base TZC and tantalum base T-111 alloys. The tests were conducted at temperatures between 1800 and 2200°F, using frequencies between 10 and 19 KHz, and A ratios (ratio of alternating to mean stress) between 0.1 and 0.65. High frequency fatigue creep measurements showed that the high frequency vibrations accelerated the creep rate in both alloys, and also accelerated a creep rate transition which occurs in conventional T-111 creep tests. Acceleration of the creep rate during the first stage of creep resulted in primary creep strains between 1 and 10% in both alloys, which was much larger than the very small (~.1%) primary creep strains seen in these alloys in isostatic creep tests.

Acceleration of second stage creep rates were measured for the TZC alloy and the variation of acceleration with temperature, frequency, and A ratio was studied. Comparison of this high frequency fatigue-creep behavior with the tensile behavior described by Raffo (5) suggested that the creep rate acceleration was caused by a negative strain rate sensitivity which is associated with a strain aging phenemonon in these materials.

The variation of the acceleration effect with temperature, frequency, and A ratio were all shown to be consistent with this hypothesis. By combining conventional analytical expressions which are normally used to characterize creep and strain aging behaviors it was possible to develop an equation relating the creep rate acceleration to each of these parameters for the TZC alloy.

BIBLIOGRAPHY

1. C. R. Honeycutt, T. F. Margin, J. C. Sawyer, and E. A. Steigerwald, "Elevated Temperature Fatigue of TZC Molybdenum Alloy Under High Frequency and High Vacuum Conditions," Trans. ASM, Vol. 60, 1967, p. 450.

2. K. D. Sheffler, J. C. Sawyer, and E. A. Steigerwald, "Mechanical Behavior of Tantalum-Base T-111 Alloy at Elevated Temperatures," Trans. ASM, Vol. 62, 1969, p. 749.

3. P. L. Raffo, "Dynamic Strain Aging in Carbide Strengthened Molybdenum Alloys," ASM/AIME Metallurgical Transactions, Vol. 1, 1970, p. 835.

4. J. W. Evans and B. W. Wilshire, "Transient and Steady State Creep Behavior of Nickel, Zinc, and Iron," Trans. AIME, Vol. 242, 1968, p. 1303.

5. F. Garofalo, C. Richmond, W. F. Domis, and F. VonGemmingen, "Stress-Time, Rate-Stress, and Rate-Temperature Relations During Large Deformations in Creep," Joint International Conference on Creep, p. 1-31, The Inst. of Mech. Engr., London, 1963.

6. J. D. Lubahn and R. P. Felgar, Plasticity and Creep of Metals, John Wiley & Sons, New York, 1961, p. 173.

TABLE 1

CHEMICAL ANALYSIS OF T-111 HEAT 650038 STUDIED IN THE PROGRAM

Weight Percent			PPM				
W	Hf	Ta	C	O	N	H	
8.6	2.0	Balance	25	100	20	2.8	Pretest
			55	19	41	9.0	Post Test

TABLE 2

CHEMICAL ANALYSIS OF TZC ALLOY

	Weight Percent				PPM		
	Ti	Zr	Mo	C	O	N	H
Heat 4230	1.35	.29	Balance	.089	N.A.	N.A.	N.A.
Heat 4345	1.24	.15	Balance	.130	19	9	2
Heat 4350	1.40	.17	Balance	.125	N.A.	N.A.	N.A.

TABLE 3

TENSILE PROPERTIES OF RECRYSTALLIZED T-111 AND TZC ALLOYS AT 2000°F (1093°C)

Material	Ultimate Strength Ksi	0.2% Yield Strength Ksi	Elongation %
T-111	62	33	27
TZC	61	24	28

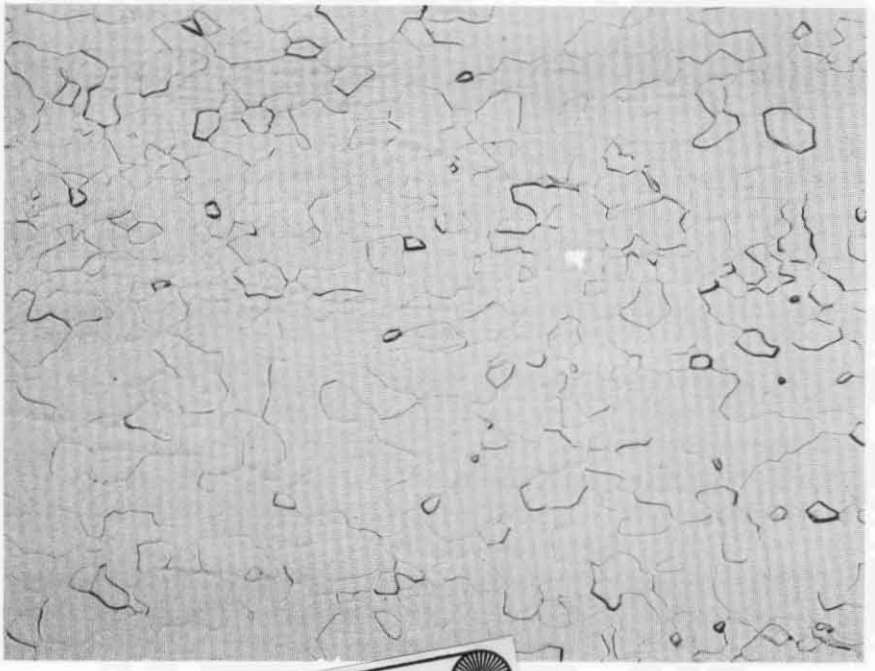

FIGURE 1. OPTICAL PHOTOMICROGRAPH OF T-111 PLATE RECRYSTALLIZED 1 HOUR AT 3000°F (1649°C). 100X

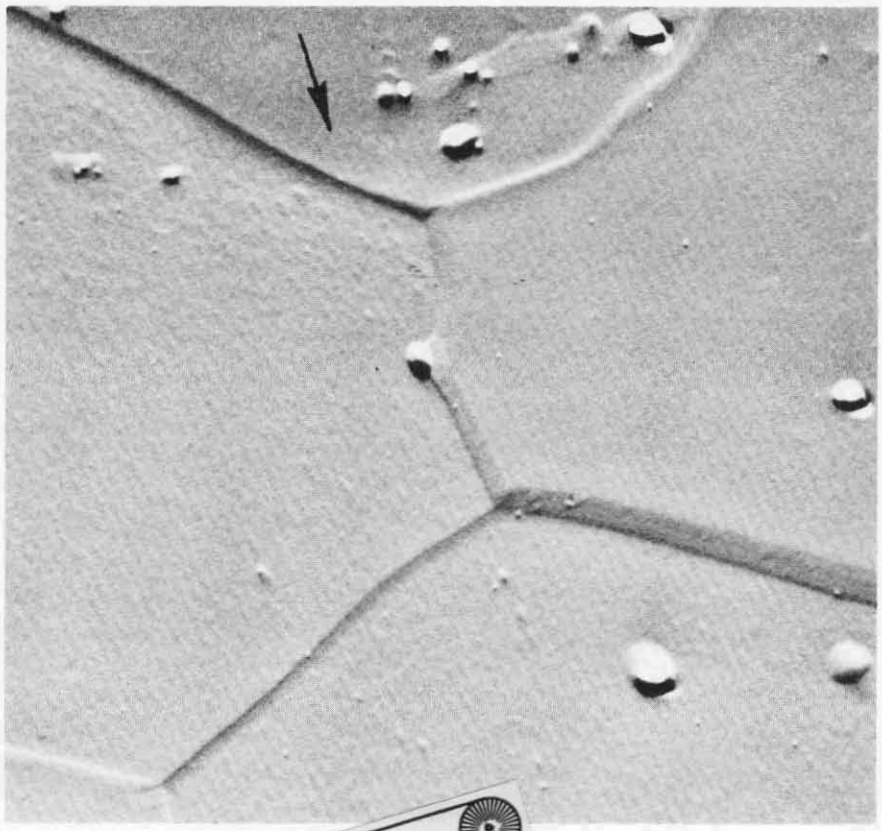

FIGURE 2. ELECTRON MICROGRAPH OF T-111 PLATE RECRYSTALLIZED 1 HOUR AT 3000°F (1649°C). TWO STAGE REPLICA (CELLULOSE-NITRATE/ CARBON). ARROW INDICATES THE DIRECTION OF CHROMIUM SHADOWING ON PRIMARY REPLICA. 7500X

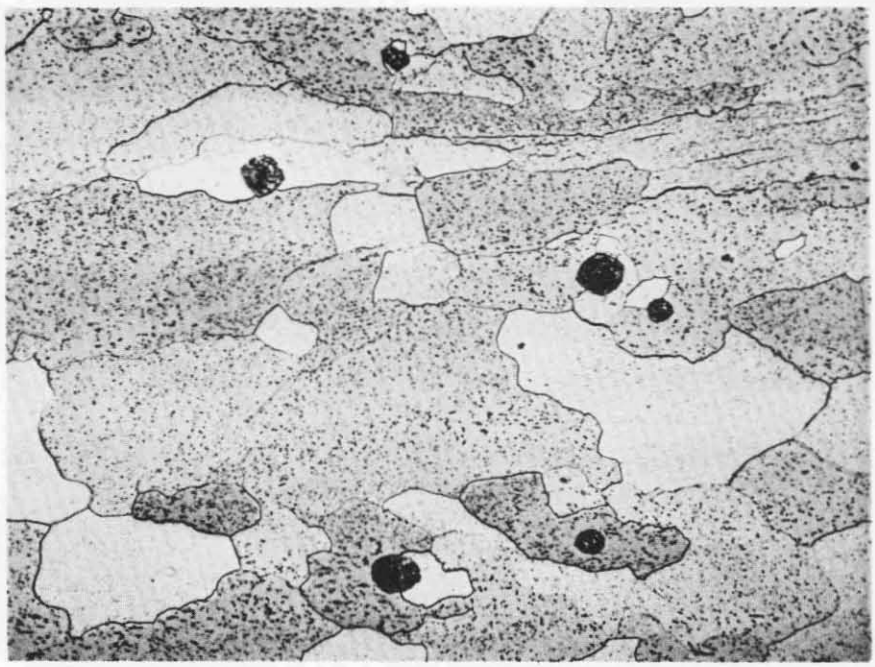

FIGURE 3. OPTICAL PHOTOMICROGRAPH OF TZC HEAT 4345 RECRYSTALLIZED 1 HOUR AT 3092°F (1700°C). 500X

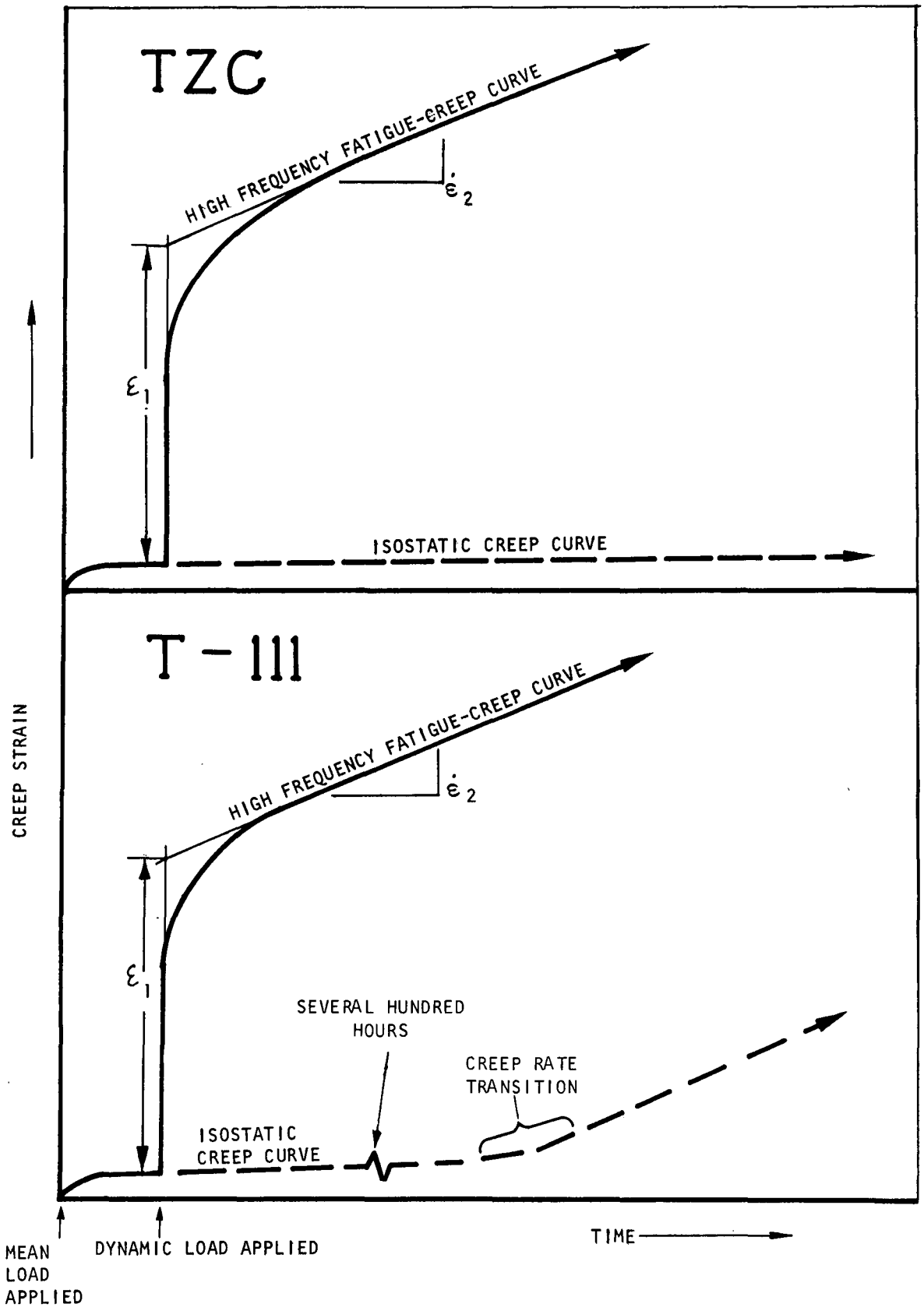

FIGURE 4. SCHEMATIC COMPARISON OF ISOSTATIC AND HIGH FREQUENCY FATIGUE CREEP BEHAVIORS.

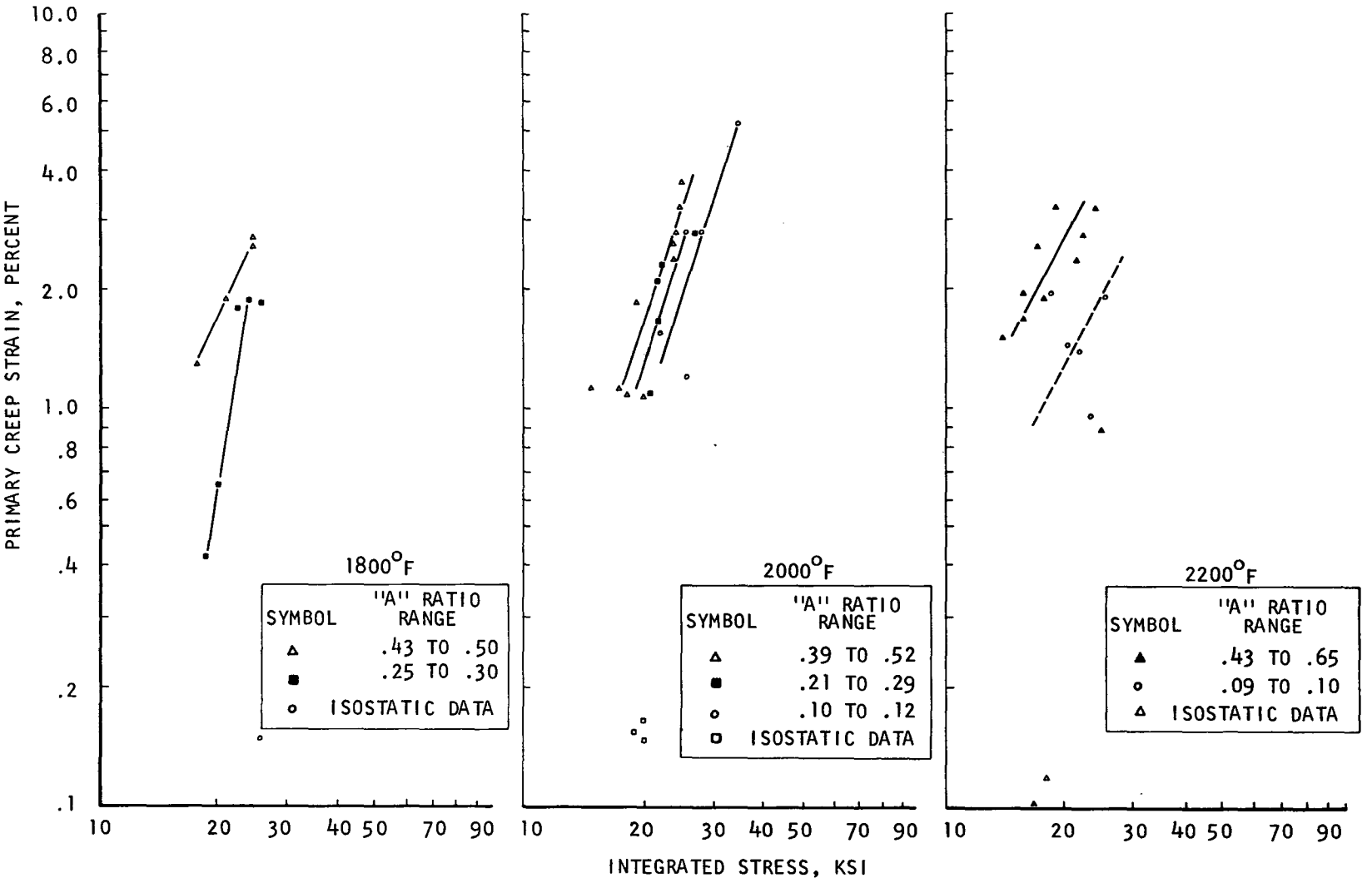

FIGURE 5. COMPARISON OF ISOSTATIC AND HIGH FREQUENCY FATIGUE-CREEP PRIMARY EXTENSIONS IN TZC ALLOY. SEE APPENDIX A FOR EXPLANATION OF THE INTEGRATED STRESS.

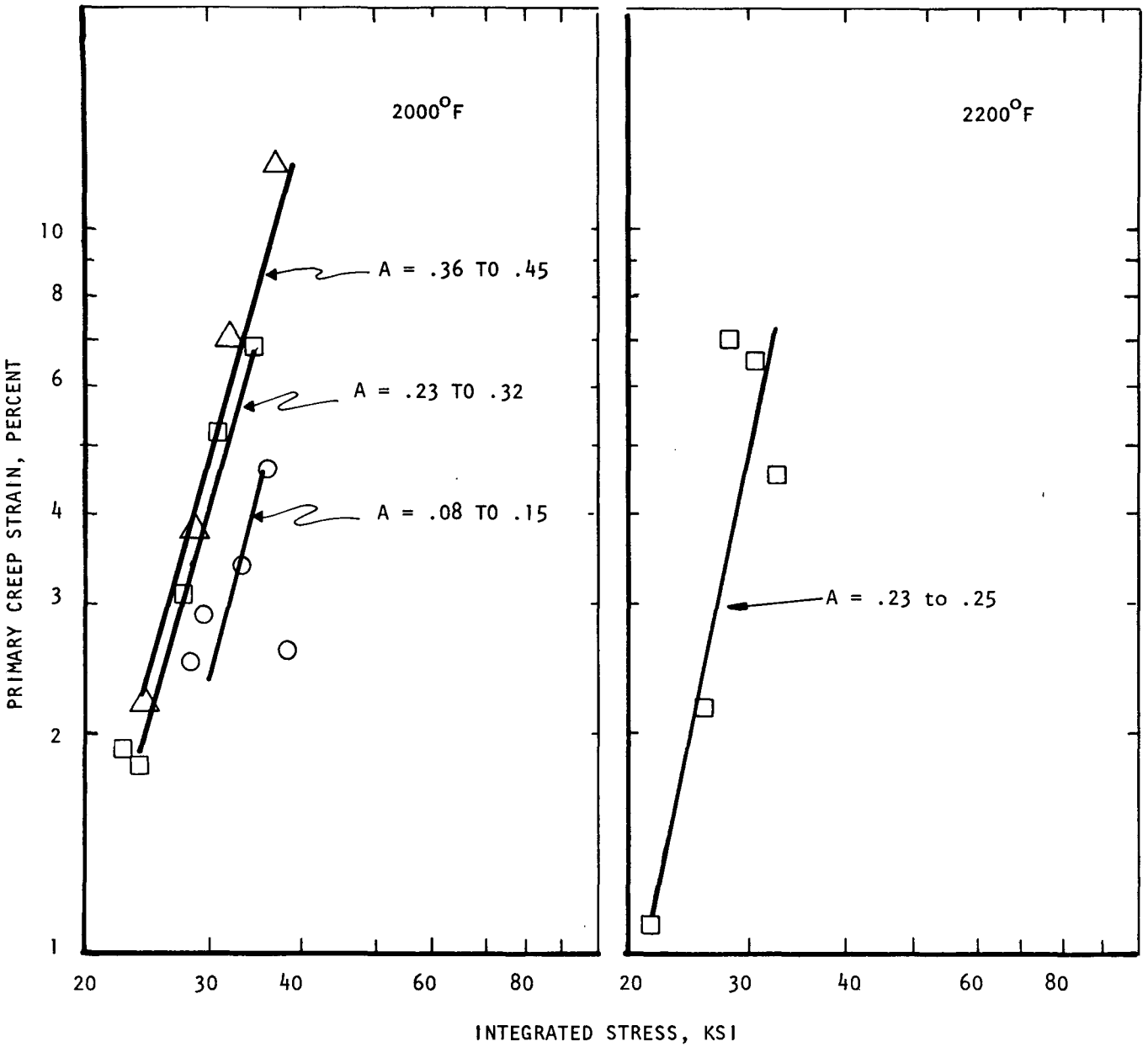

FIGURE 6. HIGH FREQUENCY FATIGUE-CREEP PRIMARY EXTENSIONS IN T-111 ALLOY. SEE APPENDIX A FOR EXPLANATION OF THE INTEGRATED STRESS.

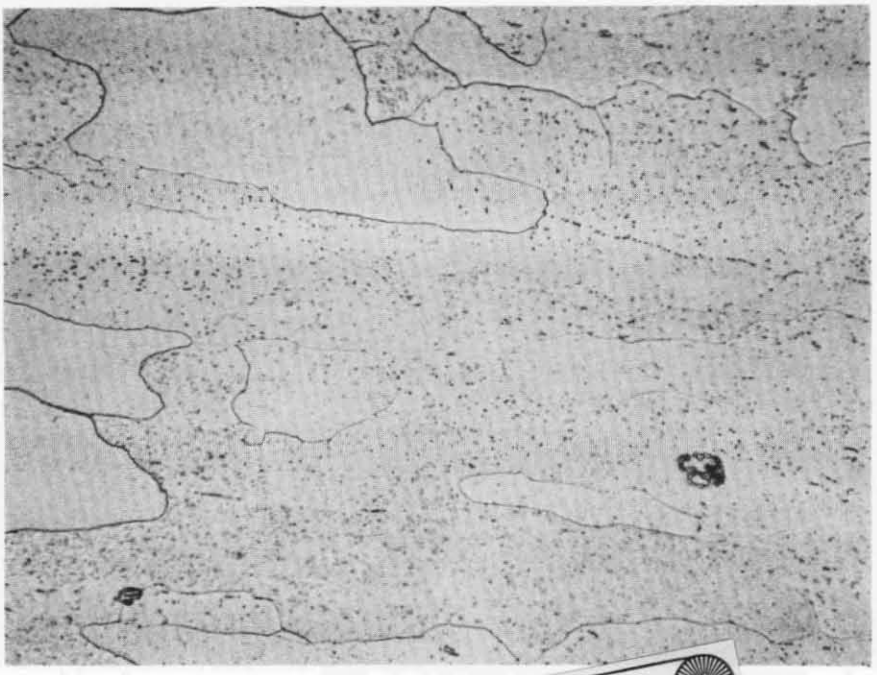

FIGURE 7. MICROSTRUCTURE OF TZC ALLOY FATIGUE TESTED 5.2 HOURS AT 2000°F, 22 KSI PEAK STRESS, A = .47, 1.96% TOTAL CREEP. 500X

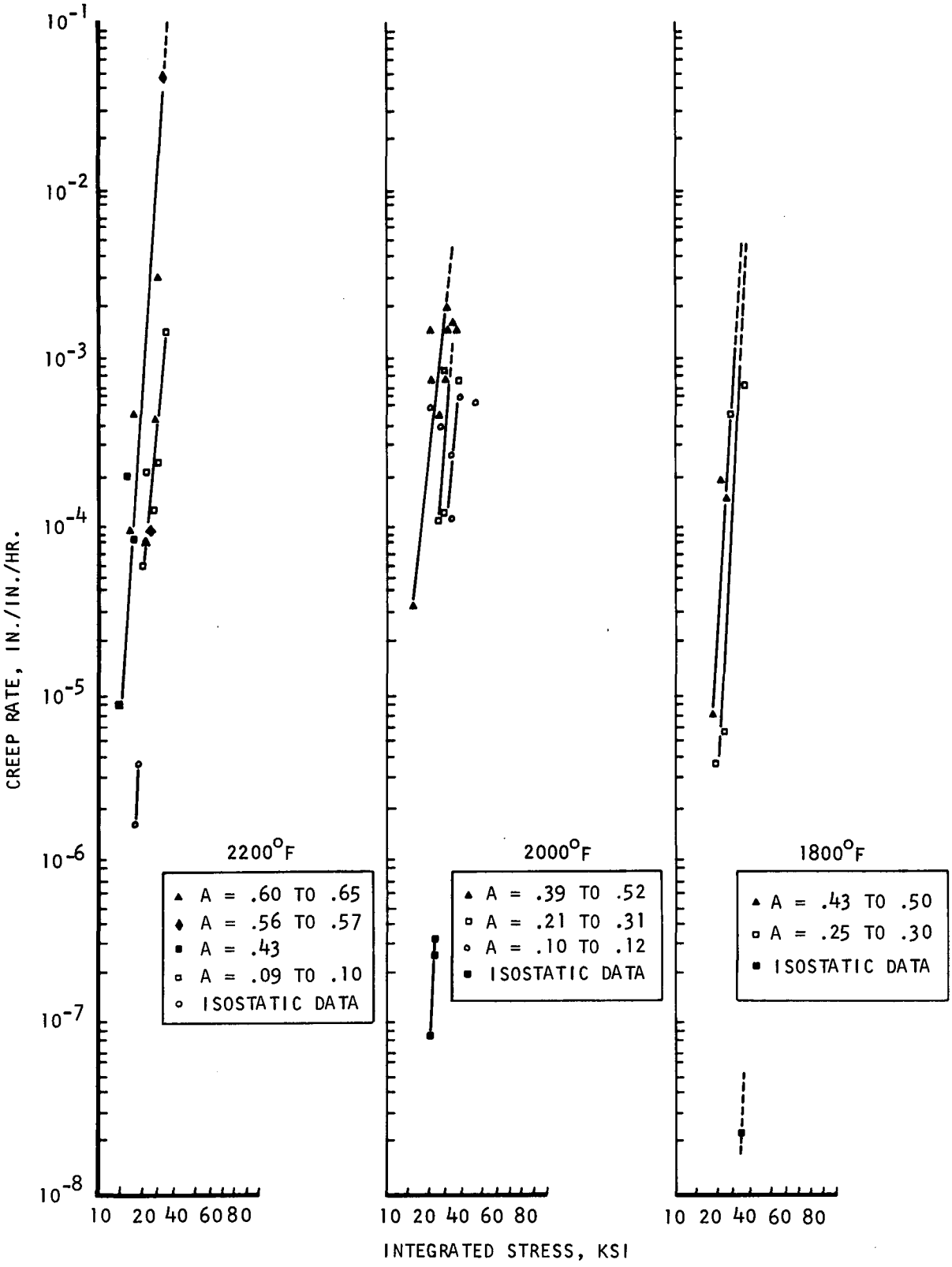

FIGURE 8. COMPARISON OF ISOSTATIC AND HIGH FREQUENCY FATIGUE CREEP RATES IN TZC ALLOY FOR DIFFERENT "A" RATIOS. SEE APPENDIX A FOR EXPLANATION OF INTEGRATED STRESS.

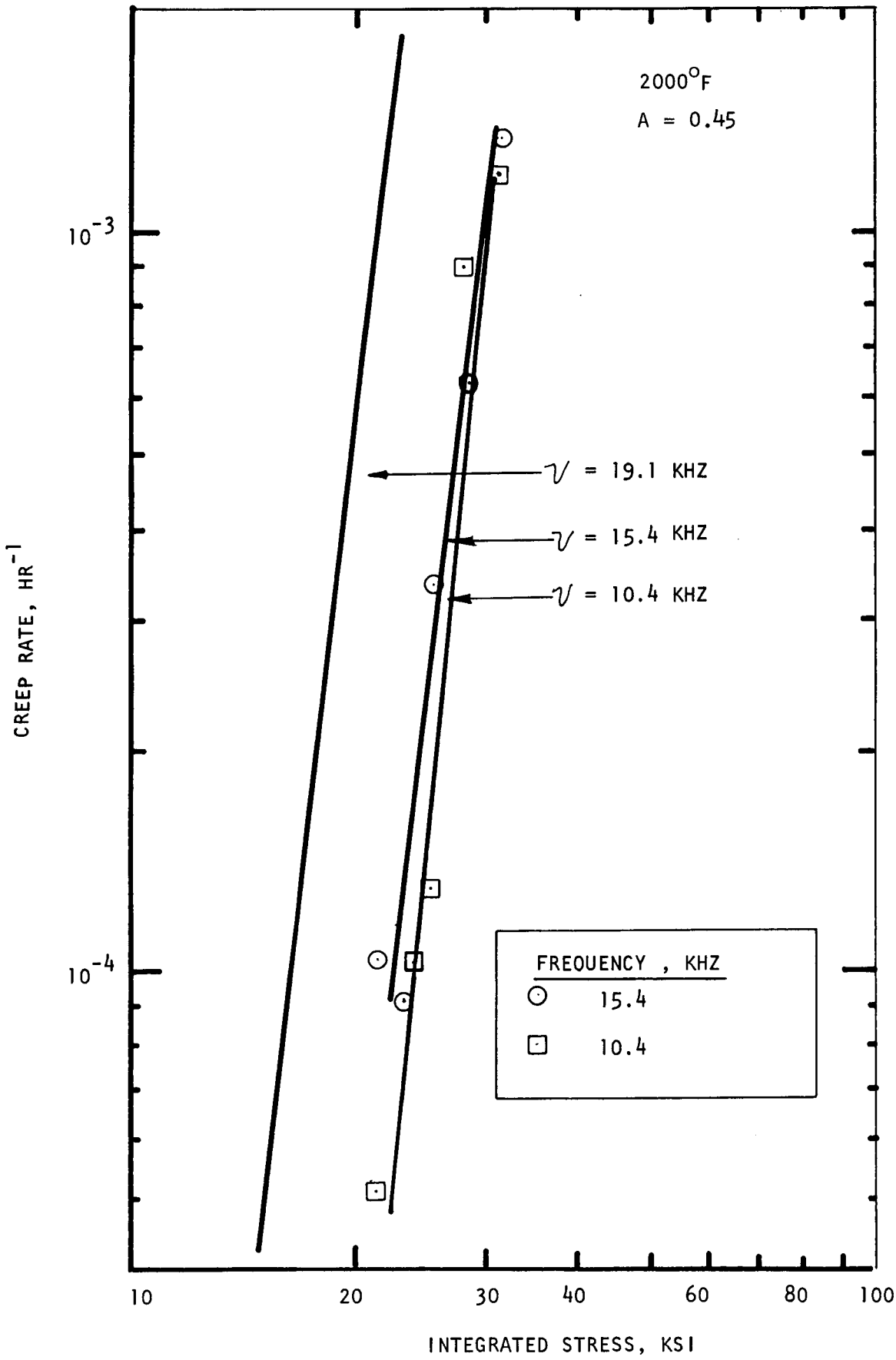

FIGURE 9. INFLUENCE OF FREQUENCY ON THE HIGH FREQUENCY FATIGUE-CREEP BEHAVIOR OF TZC ALLOY 2000°F, A = 0.45. SEE APPENDIX A FOR EXPLANATION OF INTEGRATED STRESS.

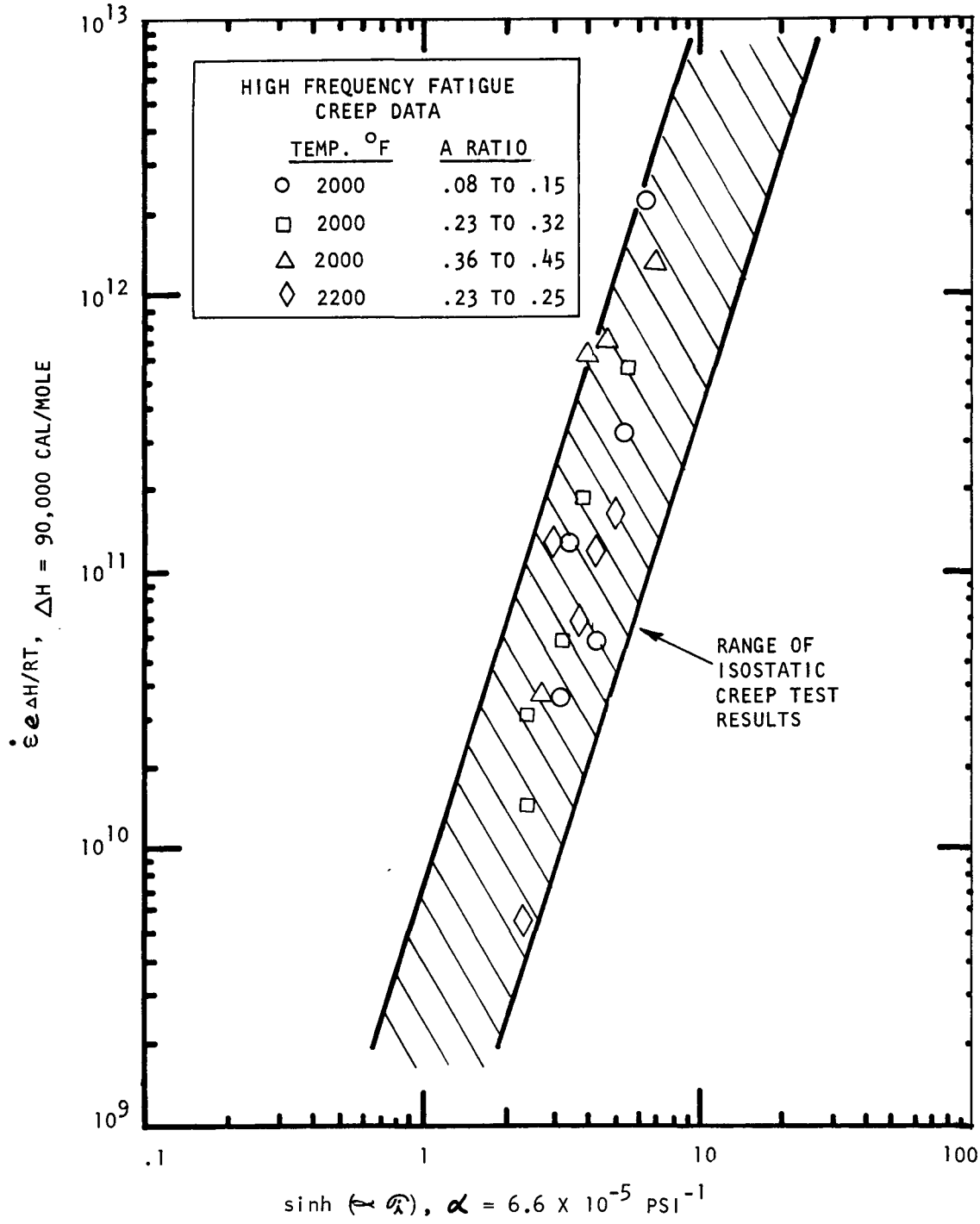

FIGURE 10. COMPARISON OF T-111 ISOSTATIC AND HIGH FREQUENCY FATIGUE STEADY STATE CREEP RATES. (SEE REFERENCE 2 FOR EXPLANATION OF THE HYPERBOLIC SINE STRESS FUNCTION AND TEMPERATURE COMPENSATED CREEP RATE.)

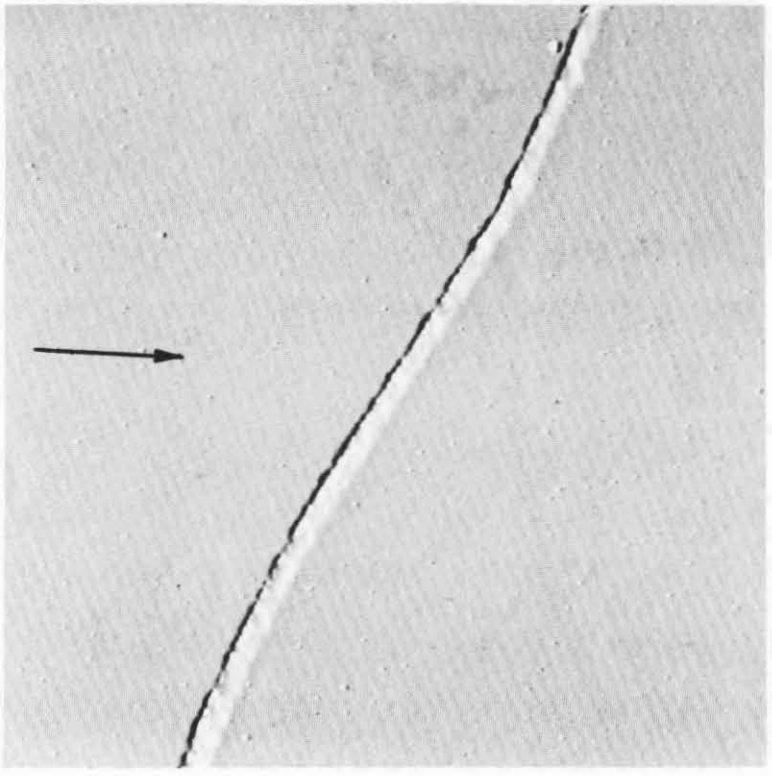

FIGURE 11. ELECTRON MICROGRAPHS SHOWING REMOVAL OF HAFNIA FROM T-111 FATIGUE TESTED 0.5 HOURS AT 2200°F, 37.5 KSI PEAK STRESS, A = 0.25, 8.6% TOTAL DYNAMIC CREEP. TWO STAGE REPLICA (CELLULOSE-NITRATE/CARBON). ARROWS INDICATE DIRECTION OF CHROMIUM SHADOWING ON PRIMARY REPLICA. 7500X

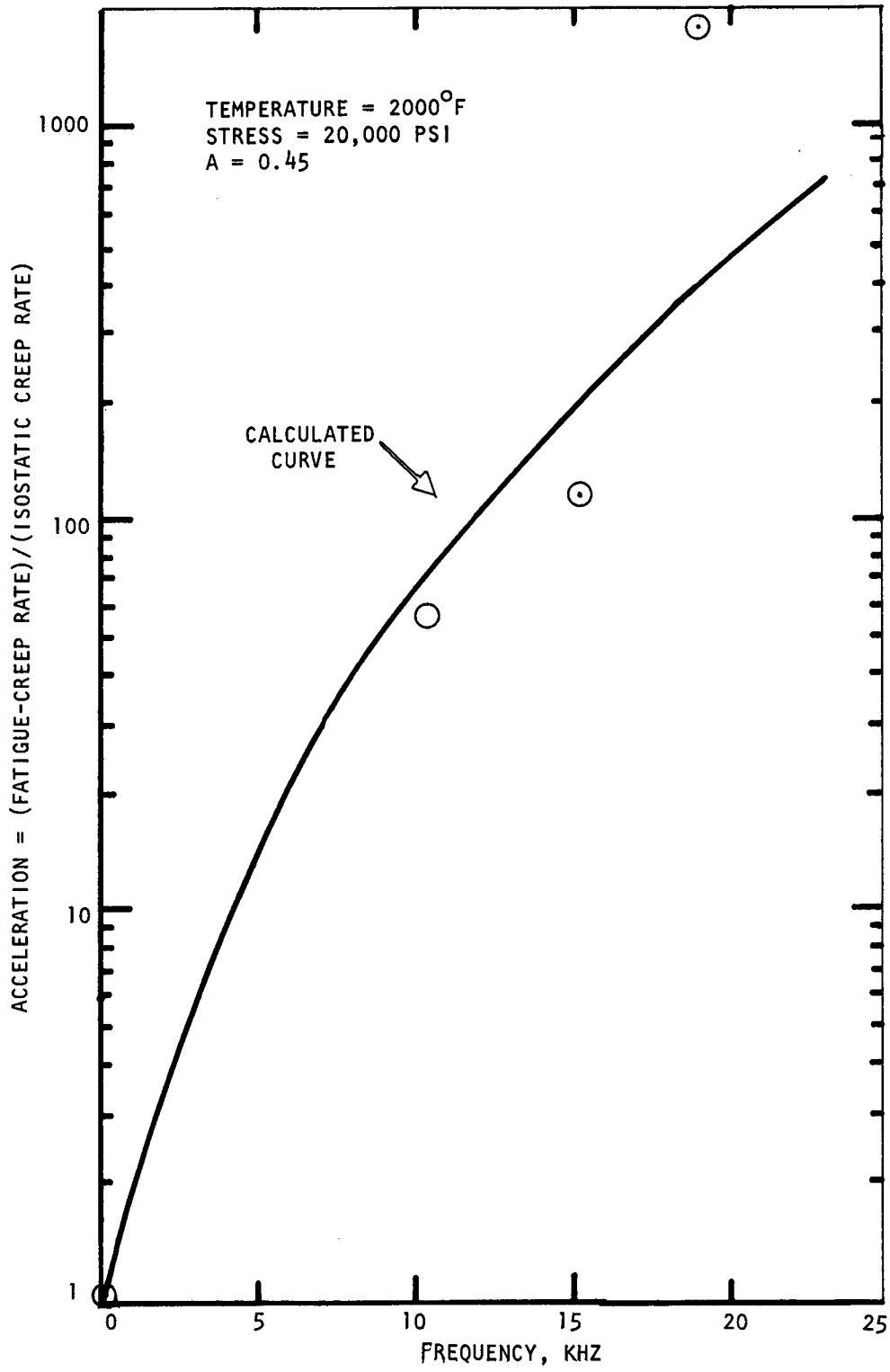

FIGURE 12. COMPARISON OF CALCULATED AND EXPERIMENTAL MEASUREMENTS OF THE INFLUENCE OF FREQUENCY ON THE CREEP RATE ACCELERATION IN TZC ALLOY.

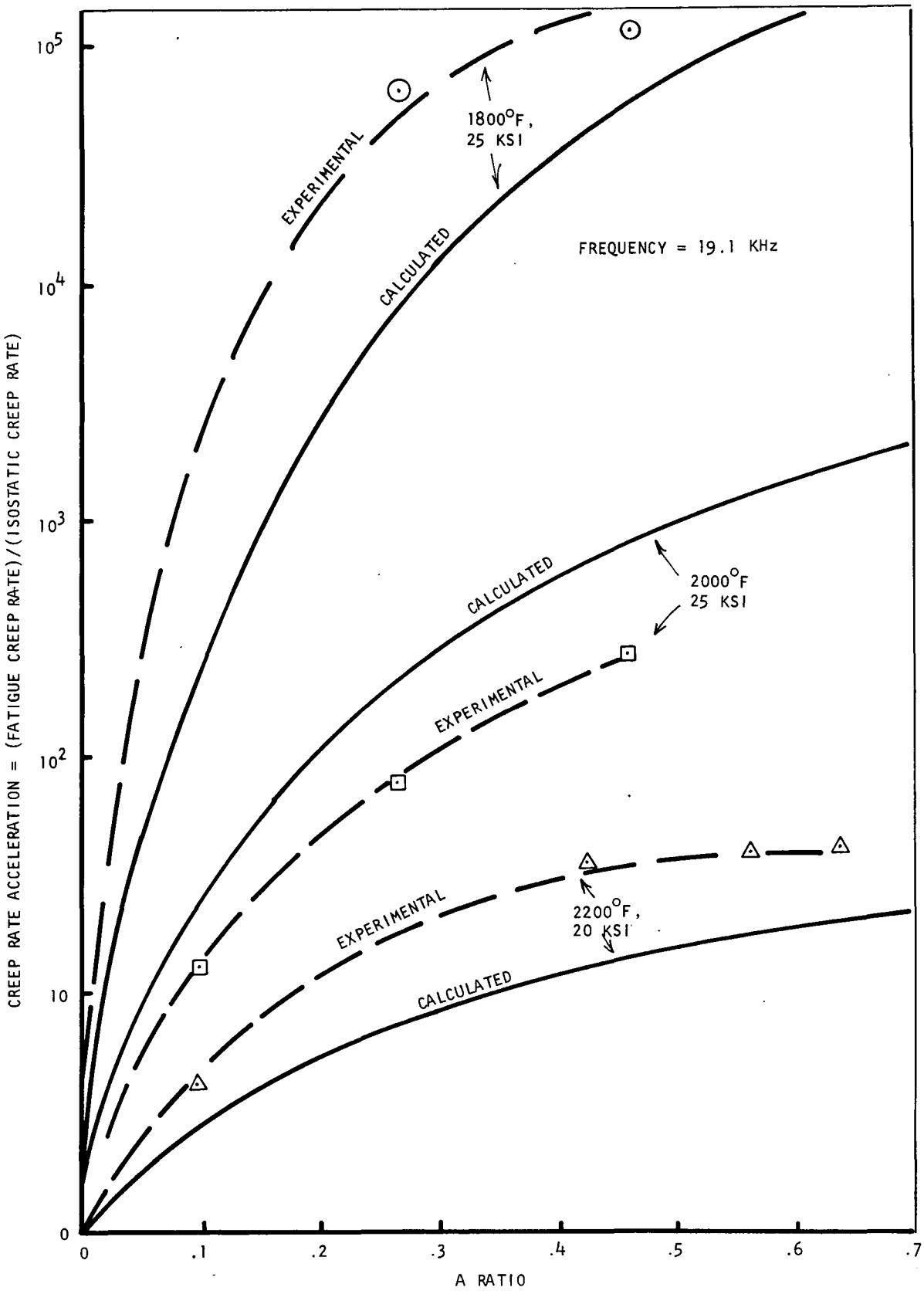

FIGURE 13. COMPARISON OF CALCULATED AND EXPERIMENTAL MEASUREMENTS OF THE INFLUENCE OF A RATIO ON THE CREEP RATE ACCELERATION IN TZC ALLOY.

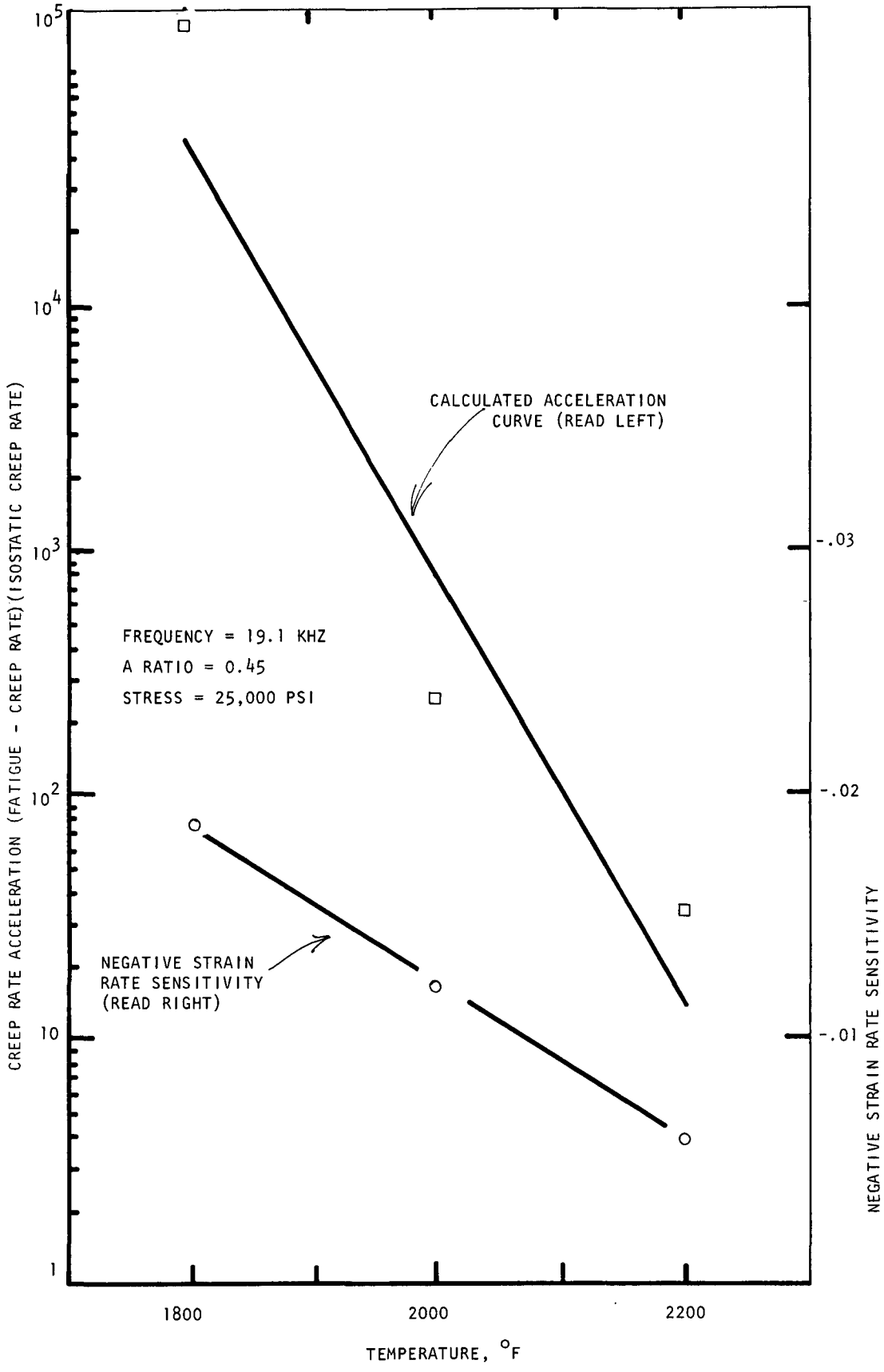

FIGURE 14. COMPARISON OF CALCULATED AND EXPERIMENTAL MEASUREMENTS OF THE INFLUENCE OF TEMPERATURE ON THE CREEP RATE ACCELERATION IN TZC ALLOY, SHOWN TOGETHER WITH EXPERIMENTAL MEASUREMENTS OF THE INFLUENCE OF TEMPERATURE ON THE NEGATIVE STRAIN RATE SENSITIVITY IN TZC ALLOY.

APPENDIX A

The purpose of this appendix is to explain the integrated stress used to compare high frequency fatigue-creep data with conventional creep results. The integrated stress is essentially a mean stress value which has been adjusted upward slightly to account for the relatively small creep rate acceleration caused by the non-linear dependence of creep rate on stress. The use of this adjusted mean stress for comparison automatically separates this relatively small stress dependence acceleration from the total acceleration measured in the fatigue-creep tests. This separation allows the strain rate softening component of the acceleration to be evaluated directly. A detailed discussion of the integrated stress calculation follows.

The stresses and strains measured in the high frequency fatigue tests are not instantaneous values but are the means of values which vary sinusoidally with time. This point is illustrated schematically in Figure A-1, which shows the relationship between the mean and instantaneous stresses, strains, and creep rates. The independent variables in the fatigue test are the mean stress and the dynamic strain range. The mean strain is a measured dependent variable while the dynamic stress is calculated from the applied dynamic strain using the relationship.

$$\sigma = E\varepsilon \qquad \text{A-1}$$

where E is the dynamic elastic modulus.

Even if no transient strengthening or weakening effects (such as strain rate softening) occurred, the instantaneous creep rate indicated in Figure A-1 would not be constant, as implied by the straight line in the illustration, but would vary with stress through each fatigue cycle. Because of the non-linear

dependence of creep rate on stress, the creep rate increases much more on the high stress half of the cycle than it decreases on the low stress half. This concept is illustrated in Figure 2, where the instantaneous creep rate has been plotted over a full fatigue cycle assuming a stress law of the form:

$$\dot{\varepsilon} \propto \sigma^N$$

The creep strain accumulated over the complete cycle (which is the area under the curve in Figure A-2) is greater than the strain which would be accumulated in the same time at the mean stress. This means that a sinusoidal fatigue cycle superimposed on the creep stress will cause some acceleration of the measured creep rate simply because of the non-linear dependence of creep rate on stress.

The integrated stress can be defined as the isostatic stress which would produce a creep rate equivalent to the time-averaged creep rate in Figure A-2. Analytical determination of the time-averaged creep rate is accomplished by integration of the instantaneous creep rate over a fatigue cycle:

$$\text{average creep rate} = \bar{\dot{\varepsilon}} = \frac{\int \dot{\varepsilon}(t)\,dt}{\int dt} \qquad \text{A-2}$$

Assuming the power law for creep, the creep rate is given as a function of time by

$$\dot{\varepsilon}(t) = c[\sigma(t)]^N = c\sigma_m^N(1+A\sin 2\pi\nu t)^N \qquad \text{A-3}$$

Substituting Equation A-3 into A-2 yields

$$\bar{\dot{\varepsilon}} = \frac{\int c\sigma_m^N(1+A\sin 2\pi\nu t)^N dt}{\int dt} \qquad \text{A-4}$$

The assignment of definite integration limits provides:

$$\bar{\dot{\varepsilon}} = \frac{c\sigma_m^N \int_o^1 (1+A\sin 2\pi\nu t)^N d(\nu t)}{\int_o^1 d(\nu t)} \qquad \text{A-5}$$

or, since the denominator in equation A-5 is unity,

$$\bar{\dot{\varepsilon}} = c\sigma_m^N \int_o^1 (1+A\sin 2\pi\nu t)^N d(\nu t) \qquad \text{A-6}$$

The integrated stress σ_i is the stress which would provide a creep rate of $\bar{\dot{\varepsilon}}$ in an isostatic test:

$$\bar{\dot{\varepsilon}} = c\sigma_i^N \qquad \text{A-7}$$

Equating expressions A-6 and A-7 provides

$$c\sigma_i^N = c\sigma_m^N \int_o^1 (1+A\sin 2\pi\nu t)^N d(\nu t) \qquad \text{A-8}$$

Dividing both sides of this equation by $c\sigma_m^N$ and taking the Nth root provides the result:

$$\sigma_i/\sigma_m = \{\int_o^1 (1+A\sin 2\pi\nu t)^N d(\nu t)\}^{1/N} \qquad \text{A-9}$$

This expression was evaluated for A ratios between zero and one using computer assisted numerical integration techniques, with the results shown in Figure A-3. A computer assisted least squares curve fitting procedure was used to show that the curve in Figure A-3 could be approximately described the the expression:

$$\sigma_i/\sigma_m = 1/(C+DA) \qquad \text{A-10}$$

in the A ratio range of 0 to .5, C and D have the values

$$C = 1.019339$$

$$D = -0.3328125$$

This expression was used to represent the σ_i/σ_m ratio in the analytical treatments in Appendix B.

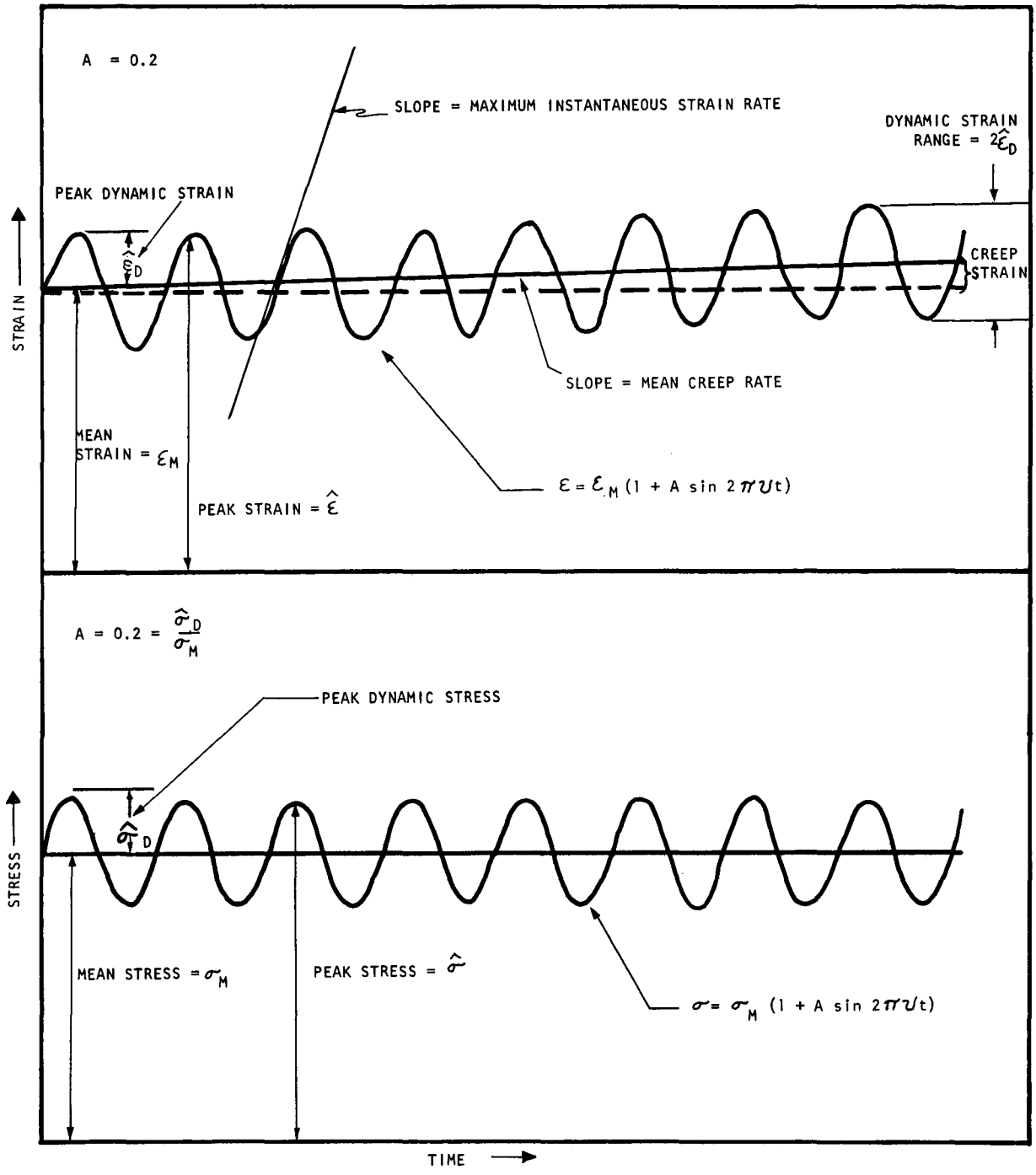

FIGURE A-1. SCHEMATIC ILLUSTRATION OF THE VARIATION OF INSTANTANEOUS AND MEAN STRESS AND STRAIN WITH TIME IN A HIGH FREQUENCY FATIGUE - CREEP TEST.

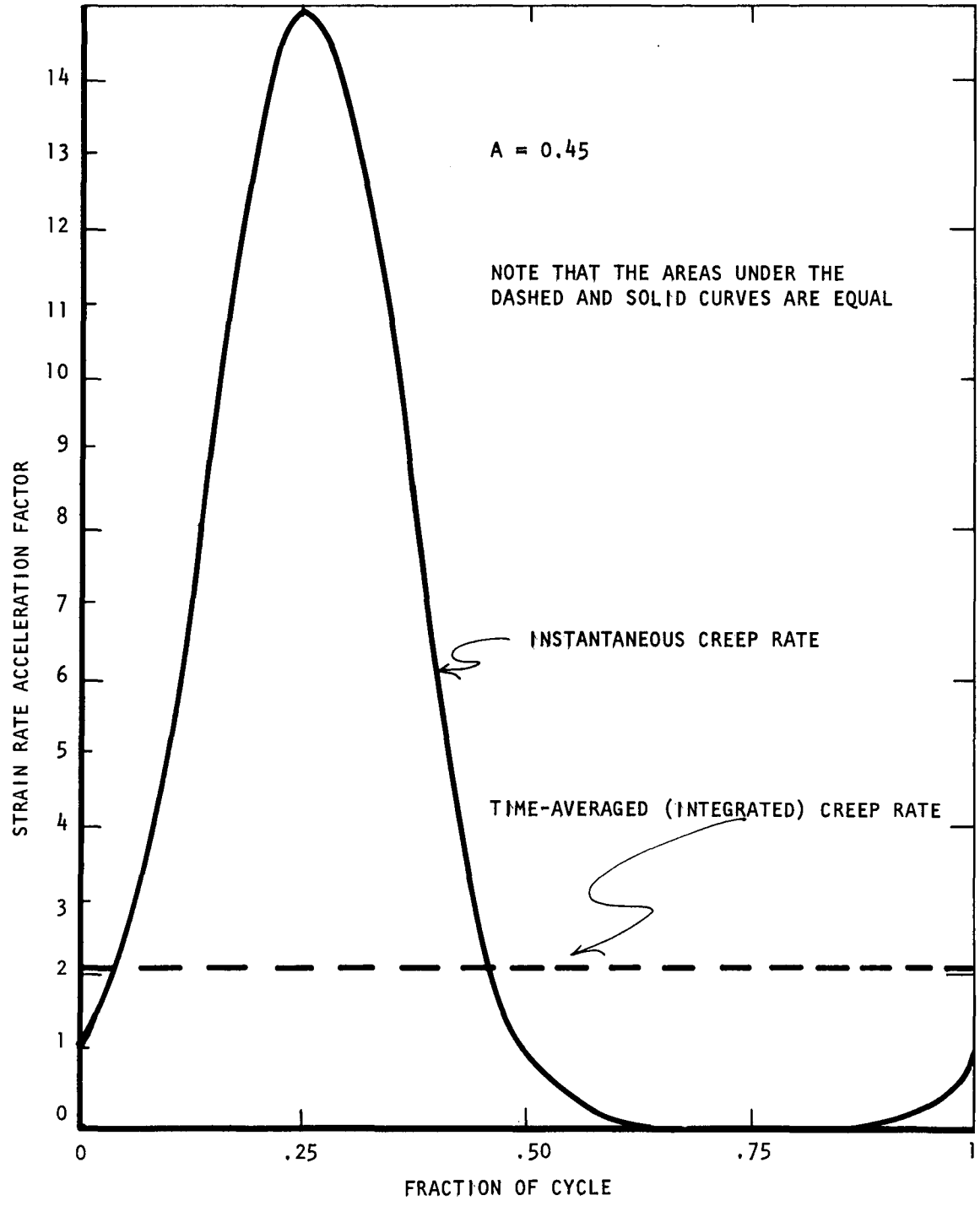

FIGURE A-2. VARIATION OF STRAIN RATE THROUGH A SINGLE FATIGUE CYCLE, NORMALIZED TO A STRAIN RATE OF ONE AT THE MEAN STRESS.

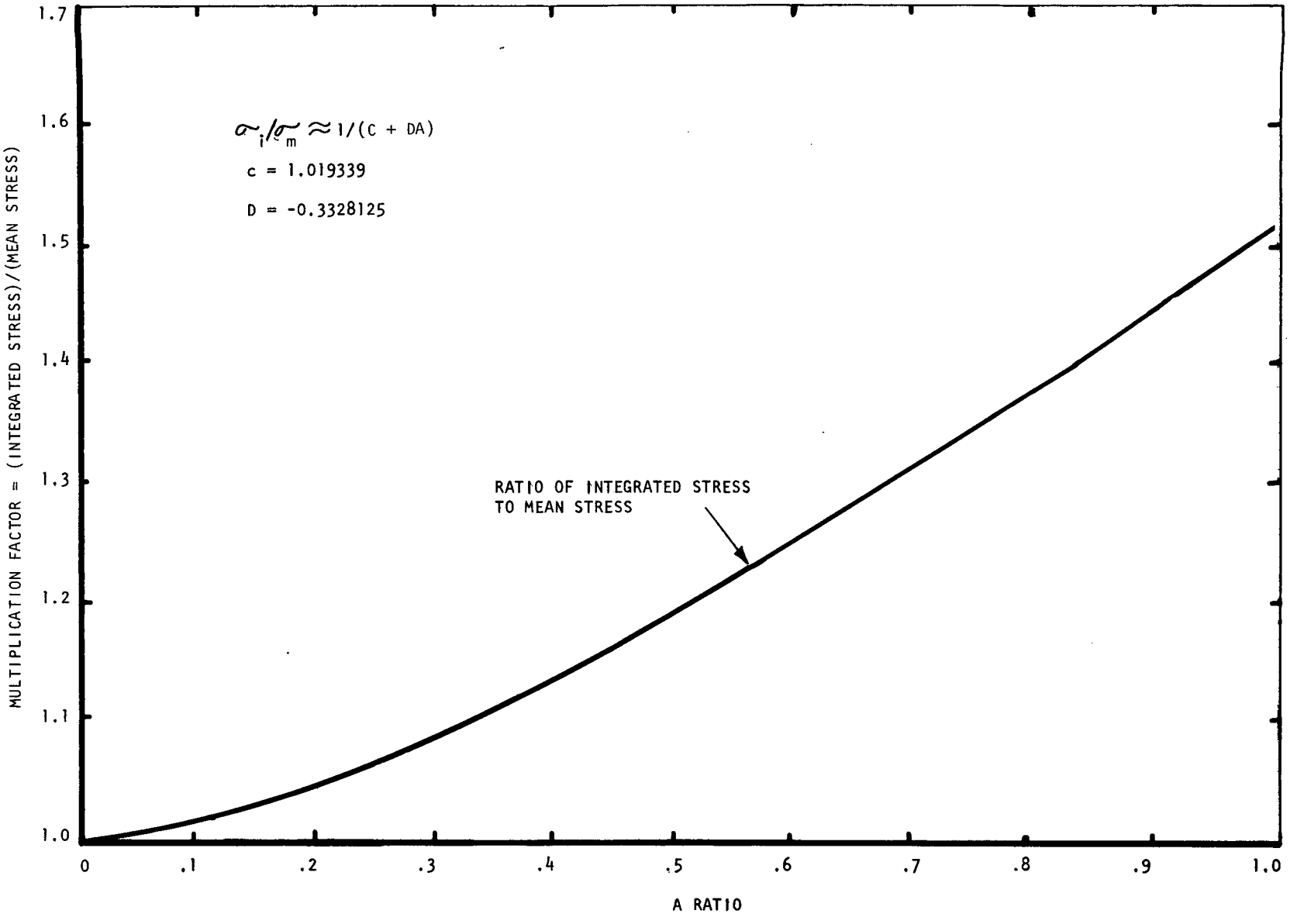

FIGURE A-3. A PLOT OF THE RATIO OF INTEGRATED TO MEAN STRESS SHOWN AS A FUNCTION OF A RATIO.

APPENDIX B

To provide additional support for the strain rate softening hypothesis an equation was developed to relate the high frequency fatigue-creep rate acceleration to frequency, temperature, and A ratio in TZC alloy. An expression given by Lubahn and Felgar (6) was used to relate flow stress (σ_f) to strain rate ($\dot{\varepsilon}$):

$$\sigma_f = K\dot{\varepsilon}^n \qquad \text{B-1}$$

Where K is a constant and n is the strain rate sensitivity. Values of the constants K and n in this equation were taken from Raffo's data (3), which are reproduced in Table B-1 and Figure B-1. The strength data in Table B-1 were plotted as a function of strain rate and the slope of the curve at each temperature was used as the n value shown in Figure B-1.

To relate creep rate to flow stress, an activation energy term was added to the conventional creep rate equation:

$$\text{creep rate} = B\sigma^N \exp[-(\Delta H + V\sigma_f)/RT] \qquad \text{B-2}$$

where B is a constant, σ is applied stress, N is the stress exponent, ΔH is the activation energy, V is the activation volume, R is the unversal gas constant, and T is absolute temperature. Combining equations B-1 and B-2 provides the expression

$$\text{creep rate} = B\sigma^N \exp[-(\Delta H + VK\dot{\varepsilon}^n)/RT] \qquad \text{B-3}$$

The $\dot{\varepsilon}$ term in equation B-3 represents the instantaneous strain rate referred to in Appendix A, which can be given by the expression

$$\dot{\varepsilon} = \dot{\varepsilon}_o + 2\pi\nu\hat{\varepsilon}_d \cos 2\pi\nu t \qquad \text{B-4}$$

Where ν is frequency, t is time, and $\hat{\varepsilon}_d$ is one-half of the dynamic strain range. The $\dot{\varepsilon}_o$ term has been added to equation B-4 so that the strain rate will approach the isostatic creep rate as ν or A approach zero. The peak dynamic strain is related to the mean strain by the A ratio:

$$\hat{\varepsilon}_d = A\varepsilon_m \qquad \text{B-5}$$

and the mean strain is related to the mean stress σ_m through the dynamic modulus E:

$$\varepsilon_m = \sigma_m/E \qquad \text{B-6}$$

The above treatment leads to the expression

$$\sigma_f = K\{\dot{\varepsilon}_o + \frac{2\pi\nu A\sigma_m}{E}\cos 2\pi\nu t\}^n \qquad \text{B-7}$$

for flow stress, which can be used in equation B-2 to provide the expression:

$$\text{creep rate} = B\{\sigma_i(C+DA)(1+A\sin 2\pi\nu t)\}^N \exp\{-[\Delta H+VK(\dot{\varepsilon}_o + \frac{2\pi\alpha\nu A\sigma_i(C+DA)}{E}\cos 2\pi\nu t)^n]/RT\} \qquad \text{B-8}$$

for creep rate. The instantaneous stress σ has been replaced with a time dependent function to represent the dynamic test conditions in equation B-8, and the mean stress has been replaced with the integrated stress expression given in Appendix A so that the calculated values will represent only the rate softening component of the acceleration. A α term has also been added to the high frequency strain rate term, which can be adjusted to compensate for variations of the n term at the extremely high strain rates involved in the high frequency fatigue testing. The average creep rate acceleration resulting from high frequency fatigue can be calculated by dividing equation B-3 into equation B-8 and integrating over a full fatigue cycle, which provides the expression:

$$\text{acceleration} = \int_0^1 (C+DA)(1+A\sin 2\pi\nu t)^N \exp\left\{\frac{VK}{RT}\left[\dot{\varepsilon}_o^{\,n} - \left(\dot{\varepsilon}_o + \frac{2\pi\alpha\nu A\sigma_i (C+DA)}{E}\cos 2\pi\nu t\right)^n\right]\right\} d(\nu t) \qquad \text{B-9}$$

for the mean acceleration due to strain rate softening.

The presence of the cosine term on equation B-9 causes a problem because it is negative over the middle half of the fatigue cycle, and therefore cannot be raised to the negative fractional power n. This problem can be handled in one of two ways. It can either be assumed that the large negative strain rates do not influence the creep rate(that is, the rate of accumulation of permanent plastic strain), or it can be assumed that the negative rates accelerate creep in exactly the same way as the positive rates. The former approach is represented analytically by breaking the integral into two parts, with the limits being -1/4 to +1/4 in the first half and +1/4 to +3/4 in the second half. The cosine term is then set equal to zero in the second integral. The latter approach is implemented by using the absolute value of cosine in equation 16. In the present treatment, it was arbitrarily assumed that the former case is correct; that is, that during the half of the cycle when the instantaneous strain rate is negative, the creep rate is exactly the same as it would be at an equivalent isostatic stress. (In practice it turned out that the difference between the two extreme cases was a factor of about 2, which is relatively small when compared with the orders of magnitude accelerations being considered.)

Computer assisted numerical integration techniques were used to evaluate equation B-9 as a function of temperature, frequency, and A ratio, with the values of the constants shown in Table B-1. The constants K and n were taken from Raffo's data, and the V and α terms were adjusted to give the

best fit of the experimental data. Results of the acceleration calculations are presented in the main text.

TABLE B-1

FLOW STRESS (KSI) OF RECRYSTALLIZED TZC ALLOY AT 5% STRAIN (AFTER RAFFO, REF. 3)

Temperature °F	Strain Rate min^{-1}						
	.002	.005	.010	.050	.100	.500	2.0
600	59.3	-	-	63.1	-	-	65.7
900	59.9	-	-	55.4	-	-	52.2
1200	61.0	-	-	54.3	-	-	-
1500	66.5	-	-	57.7	-	-	56.8
1800	68.7	-	-	67.1	-	-	61.9
2100	70.4	69.3	66.3	69.5	62.3	65.5	63.7
2400	58.2	-	-	65.4	-	-	62.7
2700	38.6	-	46.3	45.1	-	47.3	49.4
3000	-	-	-	29.2	-	-	34.9

TABLE B-2

VALUES OF HIGH FREQUENCY FATIGUE-CREEP TEST PARAMETERS USED IN THE EVALUATION OF EQUATION AS A FUNCTION OF A RATIO AND FREQUENCY

Parameter			Varying A Ratio			Varying ν
T	Temperature	°C	983	1093	1204	1093
		°F	1800	2000	2200	2000
E	Dynamic Modulus, psi		39.0×10^6	35.8×10^6	32.3×10^6	35.8×10^6
K	Flow Stress at $\dot{\varepsilon} = 1$ hour^{-1}, ksi (3)		66.9	68.1	67.7	68.1
n	Strain Rate Sensitivity (3)		-.019	-.012	-.006	-.012
σ_i	Stress Level at Which Acceleration was Experimentally Measured, Ksi		25.0	25.0	20.0	20.0
ν	Freqeuncy, KHz		19.1	19.1	19.1	-
A	Ratio		-	-	-	.45
V	$Å^3$/Atom			1.21×10^4		
$\dot{\varepsilon}_o$	Hour^{-1}			10^{-4}		
C				1.019339		
D				-0.3328125		
N				5		
α				10^{-8}		

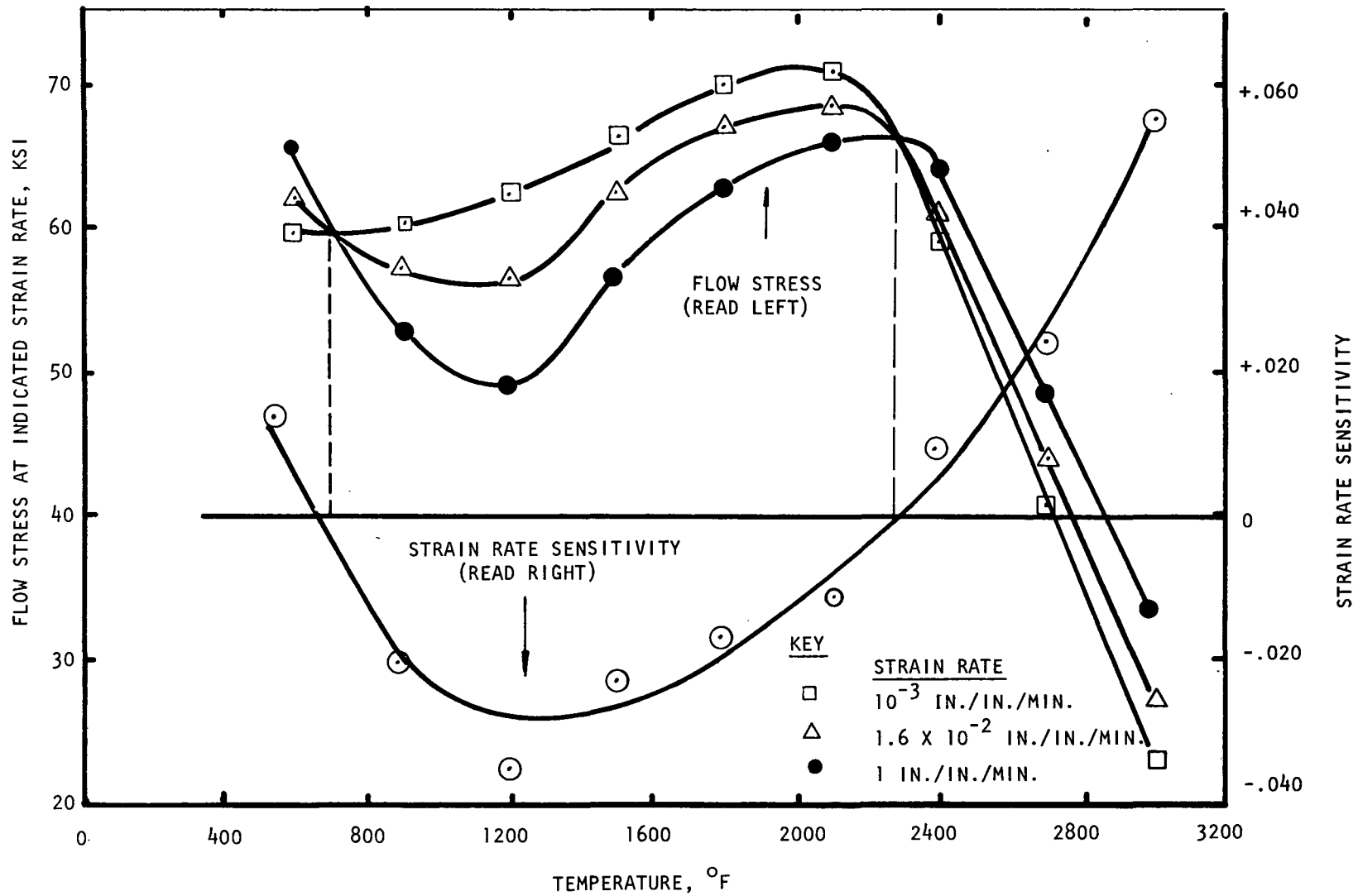

FIGURE B-1. INFLUENCE OF TEMPERATURE ON FLOW STRESS AND STRAIN RATE SENSITIVITY AT 5% STRESS IN RECRYSTALLIZED TZC ALLOY. (AFTER RAFFO, REF. 3)